DESIGN AND DEVELOPMENT OF AN UNDERACTUATED FINGER BASED ON COMPLIANT MECHANISMS

Bruno Massa and Clément Gosselin*

Département de Génie Mécanique

Université Laval

Québec, Québec, Canada, G1K 7P4

massa01@gmc.ulaval.ca, gosselin@gmc.ulaval.ca

Abstract

The objective of this paper is to present design guidelines for the development of an underactuated finger based on compliant mechanisms. The advantages related to the adoption of compliant mechanisms (the single-piece production, backlash elimination, absence of coulomb friction) represent strategic features for the finger design. A prototype of a compliant finger will be presented, the kinematics and the contact force distribution will be then analyzed using a simplified model. The results will lead to the design of a new compliant finger prototype able to apply uniform normal forces to the grasped object.

1 Introduction

Compliant mechanisms are flexible structures that deliver a desired motion by undergoing elastic deformation, as opposed to the rigid body motions of conventional mechanisms. The main advantage of compliant mechanisms is that no assembly is required for their construction. The mechanism can be constructed of one piece reducing the assembly time, the maintenance and simplifying the manufacturing processes. The adoption of compliant mechanisms can also reduce weight and eliminate wear, backlash, noise and need for lubrication [1].

Complex robotic devices such as robotic hands (see [2] for a complete survey in this field) can benefit from the use of compliant mechanisms, particularly when an adaptive behavior is needed.

*Author to whom correspondence should be addressed.

In this paper we address the problem of designing an underactuated finger based on compliant mechanisms. In general, a mechanism is said to be underactuated when it has less actuators than degrees of freedom (DOF); actuators can be replaced by elastic elements and mechanical limits. Underactuated grippers represent a particular class of robotic hands which are essentially used for grasping tasks, these devices have been designed in order to reduce both mechanical and control complexity of traditional mechanical grippers. The literature reports two different types of underactuated hands depending on the transmission system: those based on tendon transmission [3, 4, 5] and those based on link transmission [6, 7, 8]; tendon systems are generally adopted in order to minimize the device dimensions but are limited to small grasping forces, while link systems are preferred for applications in which large grasping forces are required.

The adoption of compliant mechanisms in the design of underactuated mechanical grippers represents a further reduction of the mechanical and the manufacturing process complexity. Compliant grippers have been developed in the past in order to simplify the design of traditional end-effectors, generally, when small range of motion or small forces are needed (e.g. laparoscopic grippers and micro-electro-mechanical systems) [9, 10]. Little research has been conducted on the design of compliant grippers featuring underactuated mechanisms; two examples of compliant gripper based on a differential mechanism are reported in [11, 12], where flexible pneumatic fingers have been developed. Thanks to the pneumatic actuation and to the finger flexibility, the gripper can deform to suit the shape of the objects.

In this paper the design of an underactuated finger is addressed. A first prototype based on a well known differential mechanism architecture [5] has been developed. A kinematic analysis and a static force analysis of the finger are then presented in order to synthesize a second prototype able to generate a uniform force distribution on the grasped object.

2 First Prototype

An underactuated mechanism based on tendon transmission has been chosen for the first finger prototype; this type of transmission, in fact, allows size and mass reduction of the device. The finger prototype is based on the Soft Gripper architecture [5]: a versatile gripper able to grasp objects with various shape and hold them with uniform contact forces. The original architecture

has been slightly changed in order to simplify the model and to make it suitable for the adoption of flexible joints: the Soft Gripper return cable (for the finger extension movement) has been replaced with an elastic element located in every joint. This architecture can be easily adopted for the compliant design, every pin joint and the relative spring element can be replaced with a unique flexible joint (see [13] for rigid-body replacement synthesis).

A compliant joint featuring a large bending angle represents a key point for the development of a compliant gripper. Various flexible pin joints have been developed in the past [14] and it has been pointed out that the main limitation of flexible revolute joints is their limited range of motion, in fact the elastic limit stress restricts the mobility of these joints [15]. For this reason the design of a new compliant revolute joint able to securely perform a 30 $[deg]$ rotation has been considered. Note that, for our specific application, a high motion accuracy is not required; the finger has been designed to accomplish grasp tasks and fine manipulation is not considered. In the next section the revolute compliant joint will be described and analyzed.

2.1 Compliant Joint

A "C" shaped joint (see Figure 1) has been designed in order to maximize the deflection angle, however other important characteristics such as axis drift and off-axis stiffness have been considered. A FEM software, able to solve nonlinearities due to large deflection problems, has been used

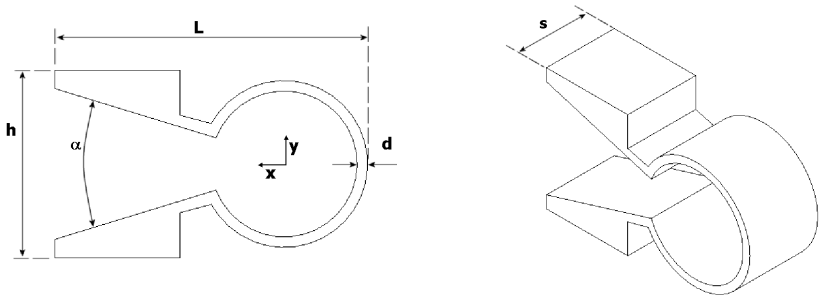

(a) (b)

Figure 1: Geometric characteristics of the compliant joint: $L = 30\,[mm]$, $\alpha = 30\,[deg]$, $d = 1\,[mm]$, $h = 18\,[mm]$ and $s = 10\,[mm]$

to analyze the joint behaviour measuring the rotational stiffness, the axis drift and the off-axis

stiffness. In all the simulations the material properties of the ABS polymer have been considered (Young's Modulus=1780 $[MPa]$, Poisson's ratio=.35, Yield stress=22.5 $[MPa]$); this material has been adopted for the development of the finger prototypes via the Fused Deposition Modeling (FDM). In Figure 2 the rotational stiffness of the joint along the z axis (k_{zz}) is reported, the compliance discontinuity is due to the contact between the two flat surfaces of the joint. If the

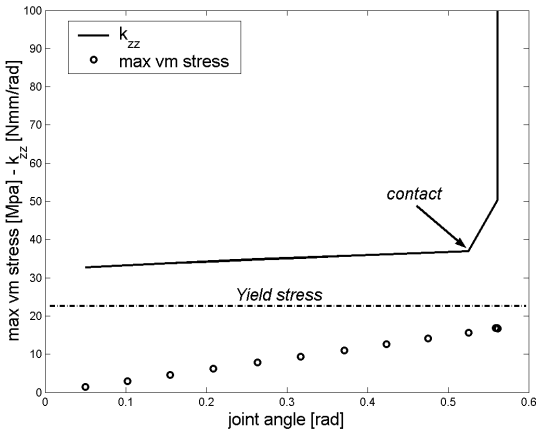

Figure 2: Rotational stiffness and max von Mises stress of the compliant joint

bending moment exceeds a certain value (18.4 $[Nmm]$) the two flat sections come in contact, preserving the joint from rupture; it is important to point out that the maximum stress remains always below the maximum allowed stress (Yield stress). Hence, the joint can securely perform a complete 30 $[deg]$ rotation thanks to the compliance discontinuity shown in Figure 2. In Table 1 the maximum and minimum values of the center of rotation drift during a complete rotation are reported. The results show a negligible axis drift, according to the requested joint precision; for

$x-axis$	$y-axis$
1.4	0.7

Table 1: Maximum axis drift (in $[mm]$) for the first compliant joint

this reason we can consider that the center of rotation remains fixed during a complete rotation, consequently, the "C" shaped joint behaves as a pin joint. Finally, the off-axis rotational stiffness for the remaining two axes (x and y-axis, k_{xx} and k_{yy} respectively) is reported in Table 2. The difference between k_{zz} and the off-axis stiffnesses k_{xx} and k_{yy} guarantees a sufficient off-axis rigidity

k_{zz}	k_{xx}	k_{yy}
34.9	88.9	152.2

Table 2: Average values of rotational stiffness and off-axis stiffness (in $[Nmm/rad]$) measured during a complete rotation for the first compliant joint

during the joint rotation.

In summary, the proposed compliant structure can replace the traditional pin joints adopted in the Soft Gripper original architecture.

2.2 Finger Design

The finger design has been realized by simply replicating the compliant joint structure and by adding a cable for the flexion movement (the extension movement is realized by means of the elasticity of the joint). Instead of replicating a three-phalanx structure adopted as in the human hand, nine compliant joints have been used in order to increase the flexibility. A hole in each compliant joint allows the cable to pass through the entire structure of the finger. The underactuated finger has been manufactured using the FDM process (see Figure 3). The FDM process represents a useful tool for compliant mechanism development; in fact, the whole finger structure can be realized in a single part and only the cable has to be added.

Several grasping tests have been carried out with this first prototype. The compliant finger shows a sufficient adaptability to the shape of several objects and the compliance discontinuity due to the contact confers a good reliability to the whole structure. On the other hand, some limitations have been noticed: (i) the finger structure is too flexible (gravitational force affects the finger configuration), (ii) hyper-extension movements of the finger reduce the feasibility of grasping tasks in which only distal phalanxes are involved (such as pinch grasps), (iii) the object tends to slip from the grasp when the power grasp cannot rely on friction forces (e.g. seizing slippery objects). In the latter case the finger is no longer able to provide multiple contact points with the object and the grasp becomes unstable (the object tends to be ejected).

The excessive flexibility will be addressed in the design of the second finger prototype by increasing the joint rotational stiffness; mechanical limits will be added in order to prevent hyper-extension;

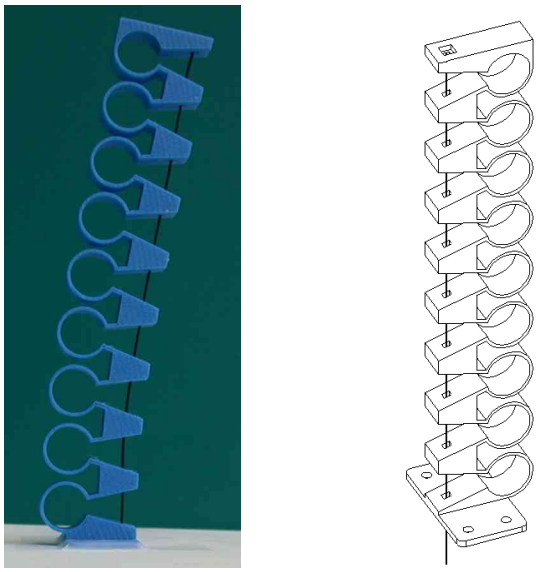

(a) (b)

Figure 3: ABS and solid model of the first compliant finger prototype

moreover, a static analysis of the finger, already presented in [16, 17], will be extended in the next section to the case of compliant fingers (where rotational stiffness cannot be neglected) and will provide the design guidelines for a compliant finger able to apply uniform normal forces to the grasped object.

3 Finger Analysis

For the finger analysis, a pseudo-rigid-body model [18] of a general compliant finger (n phalanxes) has been considered: every compliant joint has been replaced by a revolute joint and a torsional spring (the position of the joint axis and the average spring stiffness have been chosen on the basis of the FEM analysis described in section 2.1). The kinematic analysis of the finger during an unconstrained movement will be first presented, followed by the contact force analysis.

3.1 Kinematic Analysis

The kinematic analysis can be accomplished in two steps. The first step will lead to the kinematic relationship between the location of the end effector and the joint angles $\boldsymbol{\theta} = [\theta_1, \theta_2, \ldots, \theta_n]^T$. This

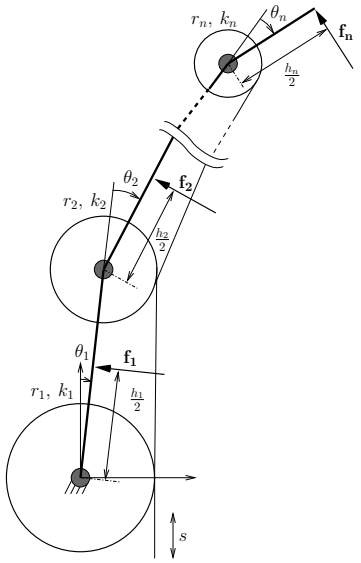

Figure 4: Finger model

step can be accomplished by the Denavit-Hartenberg method. The second step, reported below, will lead to the kinematic relationship between the joint angles $\boldsymbol{\theta}$ and the tendon displacement s during an unconstrained movement [19]. According to the notation reported in Figure 4, we can find the relation between the tendon displacement and the geometric configuration of the finger:

$$s = \mathbf{r}^T \boldsymbol{\theta} \tag{1}$$

where $\boldsymbol{r} = [r_1, r_2, \ldots, r_n]^T$ and r_i represents the distance of the cable from the center of rotation of the joint i. Given the tendon displacement, we need $n-1$ more relations to solve the kinematic problem; these equations can be found considering a quasi-static model of the finger. Let the tendon force be denoted by T, the joint torques denoted by $\boldsymbol{\tau} = [\tau_1, \tau_2, \ldots, \tau_n]^T$ and the rotational stiffness denoted by $\boldsymbol{K} = diag[k_1, k_2, \ldots, k_n]$. Applying the principle of virtual work it can be shown that:

$$\delta W = (-\tau^T - (\boldsymbol{K}\boldsymbol{\theta})^T + T\boldsymbol{r}^T)\delta\boldsymbol{\theta} \tag{2}$$

Since the system is in equilibrium the virtual work is zero for any virtual displacement $\delta\boldsymbol{\theta}$; in addition, considering that no external forces are applied to the finger, we can conclude that $\boldsymbol{\tau} = 0$. Hence we obtain:

$$T\mathbf{r} = \boldsymbol{K}\boldsymbol{\theta} \tag{3}$$

Combining these n equations with eq. 1, we can easily compute the joint angles given the tendon displacement, the remnant relation can be used to compute the cable tension associated with

the cable displacement. According to the geometrical characteristics of the first finger prototype ($n = 8$), we can say:

$$r_1 = r_2 = \ldots = r_8 = r \tag{4}$$

and

$$k_1 = k_2 = \ldots = k_8 = k \tag{5}$$

Substituting eq. 4 and eq. 5 in eq. 3 and eq 1, we obtain:

$$\theta_1 = \theta_2 = \ldots = \theta_8 = \frac{s}{8r} \tag{6}$$

and

$$T = k\frac{s}{8r^2} \tag{7}$$

3.2 Contact Force Analysis

For this analysis some assumptions have to be considered: (i) the finger link is in non-frictional point-contact with the object's edge; (ii) the contact point is located in the link midpoint; (iii) every link is in contact with the object; (iv) only one contact point per link is permitted. Let $\mathbf{f_i}$ denote a contact force acting on the link i. The relation between τ_i and $\mathbf{f_i}$ generated by the joint torques is:

$$\mathbf{f} = \mathbf{J}^{-T}\boldsymbol{\tau} \tag{8}$$

where

$$\mathbf{f} = [\mathbf{f_1}^T,\ \mathbf{f_2}^T,\ \ldots,\ \mathbf{f_n}^T]^T \tag{9}$$

$$\mathbf{J} = [\mathbf{J_1}^T,\ \mathbf{J_2}^T,\ \ldots,\ \mathbf{J_n}^T]^T \tag{10}$$

Note that $\mathbf{J_i}$ represents the Jacobian matrix associated with the contact point on link i. Thanks to the non-frictional contact assumption, we can rewrite eq. 8 in a simpler way:

$$\mathbf{f'} = \mathbf{J'}^{-T}\boldsymbol{\tau} \tag{11}$$

where

$$\mathbf{f'} = [f_1,\ f_2,\ \ldots,\ f_n]^T \tag{12}$$

represents the vector of the force magnitudes and $\mathbf{J}'$ is a squared lower triangular matrix where every element J'_{ij}, represents the moment arm measured with respect to the joint j associated with the force i. Finally, combining eq. 11 with eq. 2 we can find the expression for the contact forces.

$$\mathbf{f}' = \mathbf{J}'^{-T}(T\mathbf{r} - \mathbf{K}\boldsymbol{\theta}) \tag{13}$$

Note that the spring presence (that cannot be considered as negligible as in [16, 17]) directly affects the contact force distribution. As mentioned in the latter references the vector $\mathbf{f}'$ has to be full positive in order to prevent object ejection and have a stable contact situation. Moreover, as reported in section 2.2, we want the finger to apply uniform forces on the object; this condition can be simply written in the following form:

$$f_1 = f_2 = \ldots = f_n = f \geq 0 \tag{14}$$

Thanks to eq. 11 and the $n-1$ relations in eq. 14, we can find the torque distribution $\boldsymbol{\tau}$ for a uniform gripping finger. Note that the torque distribution depends on the finger configuration $\boldsymbol{\theta}$ and on the contact force f. This result can be considered as an extension of the results reported in [5]; in the latter reference, in fact, the torque distribution has been reported for a unique geometrical configuration ($\boldsymbol{\theta} = \mathbf{0}$). In Figure 5 the torque distribution of a finger with 6 phalanxes has been obtained for different sets of $\boldsymbol{\theta}$. The results in Figure 5 are calculated for a given contact force

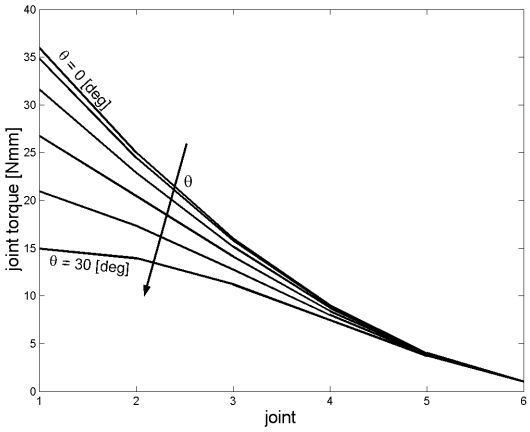

Figure 5: Torque distributions obtained for a different sets of $\boldsymbol{\theta}$

($f = 0.08\,[N]$) corresponding to $\tau_6 = 1\,[Nmm]$ and the the spring stiffness has been neglected (as in

the Soft Gripper model). Note that for $\boldsymbol{\theta} = \mathbf{0}$ we find a quadratic distribution of the joint torques as reported in [5]; this is no longer valid for other finger configurations.

4 Second Prototype

For the second prototype design the following procedure has been adopted: given the geometrical configuration of the finger $\boldsymbol{\theta}$, the dimensions of the finger, the rotational stiffness of the compliant joints $\mathbf{K}$ and the maximum and the minimum pulley radius; eq. 14 provides us $n-1$ relations that can be used to calculate the pulley radius distribution $\mathbf{r}$, the uniform grasping force magnitude f and the relative tendon tension T.

4.1 Compliant Joint

The "C" joint shape has been maintained for the second prototype and only geometric characteristics have been varied in order to increase the joint stiffness ($L = 40.5\,[mm]$, $\alpha = 35\,[deg]$, $d = 1.5\,[mm]$, $h = 27.3\,[mm]$, $s = 20\,[mm]$). The axis drift, related to a complete rotation, is showed in Table 3 and can be neglected according to the requested kinematic accuracy. The rotational stiffness and the off-axis stiffnesses are reported in Table 4 showing a greater rotational stiffness (compared to the previous joint) and an acceptable off-axis rigidity. In order to prevent

$x-axis$	$y-axis$
1.6	0.9

Table 3: Maximum axis drift (in $[mm]$) for the second compliant joint

k_{zz}	k_{xx}	k_{yy}
205.1	695.2	1128.9

Table 4: Average values of rotational stiffness and off-axis stiffness (in $[Nmm/rad]$) measured during a complete rotation for the second compliant joint

hyper-extension movements of the finger, a mechanical limit has been added in correspondence of every joint (see Figure 6). The presence of the mechanical limits is an essential requirement for grasping tasks in which only distal phalanxes are involved [8].

4.2 Finger Design

As reported in section 4 the finger synthesis is reduced now to the choice of the pulley radius distribution (distance between the cable and the center of rotation of the compliant joint). In order to limit the finger width and to respect the joint dimensions, we defined a maximum pulley radius ($r_{max} = 28\,[mm]$). Furthermore, a minimum pulley radius ($r_{min} = 10.5\,[mm]$) need to be established, r_{min} represents the the minimum distance between the cable and the center of rotation of the joint (if the cable is too close to center of rotation, the joint behaviour changes considerably and joint compression becomes predominant with respect to joint bending, consequently, the compliant joint does no longer behave as a simple revolute joint); in addition, the distal pulley radius (the smallest one) must be limited to a given value ($r'_{min} = 13\,[mm]$), r'_{min} is obtained considering the maximum cable tension needed to completely close the finger ($T_{max} = 5.7\,[N]$). In conclusion all the pulley radii have to satisfy the following relation:

$$r_{min} \leq r_i \leq r_{max} \qquad i = 1, 2, \ldots, n \tag{15}$$

For the finger design the number of compliant joints has been limited to 6 ($n = 6$) and the finger configuration has been fixed to $\theta_i = 20\,[deg]$ ($i = 1, 2, \ldots, n$). Note that, in this configuration, the finger wraps a cylindrical object with a 82 $[mm]$ diameter. In order to find the pulley radius distribution we first equal the proximal and the distal pulley radius to the maximum and the minimum value respectively:

$$\begin{cases} r_1 = r_{max} \\ r_6 = r'_{min} \end{cases} \tag{16}$$

With the latter relations and according to eq. 14, we can calculate the pulley radius distribution and the related contact force f (see Table 5).

r_1	r_2	r_3	r_4	r_5	r_6	f
28.0	24.6	21.0	17.6	14.8	13.0	0.3

Table 5: Pulley radius distribution (in $[mm]$) and the corresponding contact force (in $[N]$)

The result in Table 5 shows a low contact force between the finger and the grasped object. One possible solution to raise the contact force could be to augment r_{max} but this choice will directly

affects the finger width and, generally, the geometric characteristics of the finger ($r_{max} = 41.6\,[mm]$ is needed to double the contact force).

A more suitable solution has been adopted to solve the problem: the cable path has been changed in order to generate the desired torque distribution. One end of the cable has been connected to the distal phalanx while the other end has been fixed to the third phalanx; the cable is, now, pulled via a differential mechanisms (a simple movable pulley) that guarantees the same tension on the two cable portion (see Figure 6). According to this architecture eq. 13 can be written in this form:

$$\mathbf{f'} = \mathbf{J'}^{-T}(T\mathbf{r} + T_b\mathbf{r_b} - \mathbf{K}\boldsymbol{\theta}) \tag{17}$$

where T_b represents the tension in the second cable portion (from the third link to the differential mechanism) and $\mathbf{r_b} = [r_{1b}, r_{2b}, r_{3b}, 0, 0, 0]^T$, where r_{ib} stands for the distance between the cable and the center of rotation of the i joint. Thanks to the differential mechanism we can say:

$$T = T_b \tag{18}$$

As reported in Table 6, the proposed architecture allows the increment of the grasping force without varying the finger dimensions.

r_1/r_{1b}	r_2/r_{2b}	r_3/r_{3b}	r_4	r_5	r_6	f
28.0/25.0	28.0/15.9	23.8/10.5	25.2	17.8	13.0	0.9

Table 6: pulley radius distribution (in $[mm]$) and the corresponding contact force (in $[N]$)

The pulley radius distribution reported in Table 6 has been adopted for the second finger prototype that has been manufactured using the FDM process (see Figure 6).

The new prototype shows a greater stiffness (gravitational force does not affect the finger configuration); the mechanical limits allows more stable pinch grasps and finally, the cable path guarantees uniform grasping force distribution avoiding object ejection.

5 Conclusions

This paper has presented the design and the analysis of an underactuated finger based on compliant mechanisms able to apply uniform contact force to the grasped object. The finger design is based

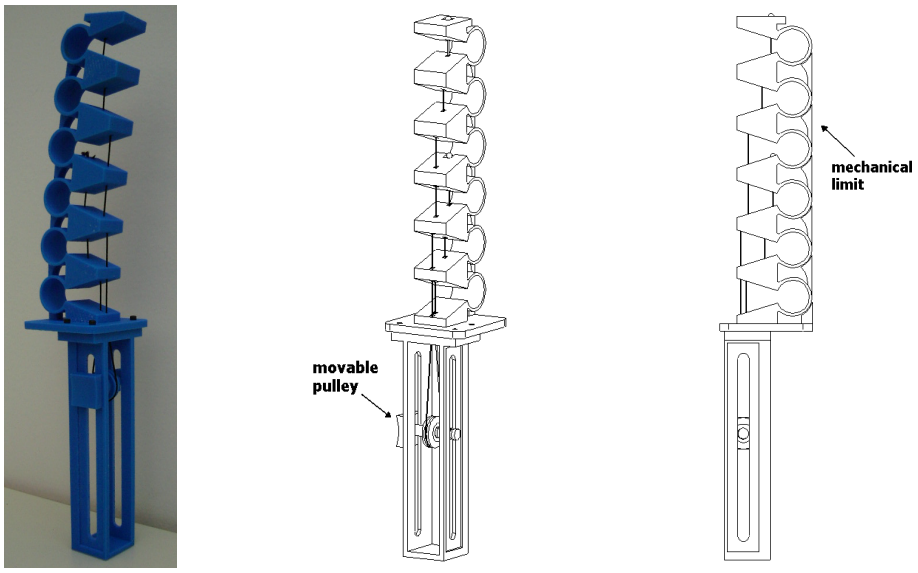

(a) (b) (c)

Figure 6: ABS and solid model of the second compliant finger prototype

on the Soft Gripper architecture [5] and the analysis reported in section 3.2 can be considered as an extension of the results reported in the latter reference.

The work reported in this paper aims at demonstrating that underactuated fingers can benefit from the use of compliant mechanisms. In comparing the underactuated finger based on compliant mechanisms to conventional underactuated finger consisting of rigid links, some observations can be made: (i) due to the uniform distribution of eight compliant joints along the finger structure, the adaptability is greater in the compliant finger than in the traditional ones, (ii) the compliant finger is more compact and reliable than the traditional ones. However some drawbacks are present: (i) the compliance of the finger cannot be varied and is strictly related to the material choice, (ii) during a general grasping task energy is stored in the compliant joints reducing the maximum allowable grasping force. Despite these limitations, the adoption of compliant mechanisms in the design of underactuated mechanical grippers represents a strategic feature for the development of lighter and simpler grasping devices.

References

[1] Smith S. T. *Flexures: Elements of Elastic Mechanisms*. Gordon and Breach Science Publishers, 2000.

[2] Bicchi A. Hands for dexterous manipulation and robust grasping: A difficult road toward simplicity. *IEEE Transaction on Robotics and Automation*, 16(6):652–662, 2000.

[3] Massa B., Roccella S., Carrozza M. C., and Dario P. Design and development of an underactuated prosthetic hand. *Proceedings of IEEE International Conference on Robotics and Automation*, 2002.

[4] Crisman J. D., Kanojia C., and Zeid I. Graspar: A flexible, easily controllable robotic hand. *IEEE Robotics and Automation Magazine*, pages 32–38, 1996.

[5] Hirose S. and Umetani Y. The development of Soft Gripper for the versatile robot hand. *Mechanism and Machine Theory*, 13:351–359, 1978.

[6] Bartholet S. J. Reconfigurable end effector. U. S. Patent 5.108.140, 1992.

[7] Crowder R. M. An anthropomorphic robotic end effector. *Robotics and Autonomous Systems*, 7:253–268, 1991.

[8] Laliberté T. and Gosselin C. M. Development of a three-dof underactuated finger. *Proceedings of CCToMM Symposium on Mechanisms, Machines, and Mechatronics*, 2001.

[9] Herder J. L. and van den Berg F. P. A. Statically balanced compliant mechanisms (SBCM'S), an example and prospects. *Proceedings of ASME Design Engineering Technical Conferences*, 2000.

[10] Haddab Y., Chaillet N., and Bourjault A. A microgripper using smart piezoelectric actuators. *Proceedings of IEEE/RSJ International Conference on Intelligent Robots and Systems*, 2000.

[11] Sozumori K. Elastic materials producing compliant robots. *Robotics and Autonomous Systems*, 18:135–140, 1996.

[12] Stone R.S.W. and Brett P.N. A flexible pneumatic actuator for gripping soft irregular shaped objects. *Proceedings of IEE Colloquium on Innovative Actuators for Mechatronic Systems*, 1995.

[13] Howell L. L. and Midha A. A method for the design of compliant mechanisms with small-length flexural pivots. *ASME Journal of Mechanical Design*, 116(1):280–290, 1994.

[14] Moon Y. M., Trease B. P., and Kota S. Design of large displacement compliant joints. *Proceedings of ASME Design Engineering Technical Conferences*, 2002.

[15] Fettig H., Wylde J., Hubbard T., and Kujath M. Simulation, dynamic testing and design of micromachined flexible joints. *Journal of Micromechanics and Microengineering*, 11:209–216, 2001.

[16] Birglen L. and Gosselin C. M. Kinetostatic analysis of underactuated fingers. *IEEE Transactions on Robotics and Automation*. accepted for publication.

[17] Birglen L. and Gosselin C. M. On the force capabilities of underactuated fingers. *Proceedings of IEEE International Conference on Robotics and Automation*, 2003. accepted for publication.

[18] Howell L. L. *Compliant Mechanisms*. John Wiley & Sons, Inc., 2001.

[19] Tsai L. W. *Robot Analysis: The Mechanics of Serial and Parallel Manipulators*. John Wiley & Sons, Inc., 1999.